Journal of Solid State Chemistry 184 (2011) 2731–2737

Contents lists available at ScienceDirect

Journal of Solid State Chemistry

journal homepage: www.elsevier.com/locate/jssc

# Metal-rich phosphides $RE_5Ir_{19}P_{12}$ with $Sc_5Co_{19}P_{12}$ type structure

Ulrike Pfannenschmidt, Ute Ch. Rodewald, Rolf-Dieter Hoffmann, Rainer Pöttgen *

*Institut für Anorganische und Analytische Chemie, Universität Münster, Corrensstraße 30, D-48149 Münster, Germany*

ARTICLE INFO

*Article history:*
Received 11 April 2011
Received in revised form
25 July 2011
Accepted 31 July 2011
Available online 5 August 2011

*Keywords:*
Phosphides
Crystal chemistry
Metal-rich compounds
Metal-flux synthesis

ABSTRACT

The iridium-rich phosphides $RE_5Ir_{19}P_{12}$ ($RE$=Sc, Y, La–Nd, Sm–Lu) with $Sc_5Co_{19}P_{12}$ type structure, space group $P6\bar{2}m$ were synthesized by solid state reactions of the elements in tantalum crucibles. Well shaped single crystals were obtained in bismuth fluxes. All phosphides were characterized on the basis of X-ray powder data. The structures of $RE_5Ir_{19}P_{12}$ with $RE$=Sc, La, Ce, Dy, Er, Tm, and Yb were refined from single crystal diffractometer data. The complex structure of these phosphides can be described by an intergrowth of simpler $ThCr_2Si_2$ and SrPtSb related slabs. Striking structural motifs of the $RE_5Ir_{19}P_{12}$ structures are slightly distorted tricapped trigonal prisms of the metal atoms around the phosphorus atoms. The iridium and phosphorus atoms build up three-dimensional $[Ir_{19}P_{12}]$ polyanionic networks (230–286 pm Ir–P and 282–296 pm Ir–Ir in $La_5Ir_{19}P_{12}$) which leave cavities of coordination numbers 16 and 15 for the rare earth atoms.



## 1. Introduction

The ternary systems $RE$–$T$–P ($RE$=rare earth element, $T$=transition metal) are characterized by a large variety of metal-rich phosphides $RE_xT_yP_z$ with metal–to–phosphorus ratios of 2:1 [1–5]. Representative series are $RET_5P_3$, $RE_2T_{12}P_7$, $RETP$, $RE_7T_{17}P_{12}$, $RE_6T_{20}P_{13}$, and $RE_5T_{19}P_{12}$. A complete overview on the crystal chemistry of this interesting subgroup of metal phosphides is given in [1,5]. The geometrical building principles are summarized in [2,6,7].

A remarkable crystal chemistry occurs for the $Sc_5Co_{19}P_{12}$ [8] type compounds. Besides a variety of $RE_5T_{19}P_{12}$ phosphides with different rare earth and transition metals [8–19], also $Zr_5Co_{19}P_{12}$ [20] and the alkaline earth compounds $Ca_5T_{19}P_{12}$ ($T$=Rh, Ir) [21] have been reported. These results show that such metallic phosphides have certain flexibility in the valence electron concentration. However, $Th_5Fe_{19}P_{12}$ [22] and $Yb_5Ni_{19}P_{12}$ [23] with the same composition have a different connectivity pattern of the distorted, phosphorus centered trigonal prisms.

$Sr_5Mg_{19}Ge_{12}$ [24] and the tetralides $M_{5+x}Mg_{18-x}E_{13}$ ($M$=Sr, Ba; $E$=Si, Ge) [25] show small homogeneity ranges on the alkaline earth positions, but they can be described as electron precise Zintl compounds, e. g. $(5Sr^{2+})(19Mg^{2+})(12Ge^{4-})$. Here the magnesium atoms fill the transition metal sites, leading to a different bonding pattern. Inverting the polarities, the salt-like compound $Ba_{12}F_{19}Cl_5$ [26] and the solid solution $Ba_{12}F_{19}Cl_\delta Br_{5-\delta}$ [27] have been reported.

In continuation of our systematic phase analytical studies of the $RE$–Ir–P systems [28–32] we obtained the series of $RE_5Ir_{19}P_{12}$ ($RE$=Sc, Y, La–Nd, Sm–Lu) phosphides. The crystal growth conditions and structure refinements are discussed herein.

## 2. Experimental

### 2.1. Synthesis

Single crystals of the metal-rich phosphides $RE_5Ir_{19}P_{12}$ ($RE$=Sc, La, Ce, Dy, Er–Yb) were prepared by a bismuth flux technique [33]. Starting materials were pieces of scandium, lanthanum, cerium, dysprosium, erbium, thulium, and ytterbium (La and Ce by Sigma Aldrich, 99.9%; Sc, Dy, Er–Yb by Smart Elements, >99.9%), iridium powder (Heraeus, >99.9%), red phosphorus (Hoechst, Knapsack, ultrapure) and bismuth shots (ABCR GmbH, >99.99%). Pieces of the rare earth metals, iridium powder, red phosphorus and bismuth shots were mixed in molar ratios of 1:2:2:30 (Sc:Ir:P:Bi) for the scandium compound and 1:2:2:60 ($RE$:Ir:P:Bi) for all other compounds. The samples were sealed in evacuated silica tubes, which were then placed in a muffle furnace. The temperature was first raised to 770 K at a rate of 20 K/h and kept for 24 h. Subsequently the samples were heated to 1320 K at a rate of 50 K/h, kept at that temperature for 100 h, followed by slow cooling to 970 K at a rate of 2 K/h and further to 570 K at a rate of 4 K/h. The samples were finally quenched in air and the excess bismuth flux was slowly dissolved with a 1:1 molar mixture of glacial acetic acid (VWR International) and $H_2O_2$ (ACROS, 35%). The resulting samples were washed with demineralized water. The reaction products consisted of partially intergrown, needle-shaped

* Corresponding author. Fax: +49 251 83 36002.
*E-mail address:* pottgen@uni-muenster.de (R. Pöttgen).

0022-4596/$ - see front matter © 2011 Elsevier Inc. All rights reserved.
doi:10.1016/j.jssc.2011.07.045

crystals with metallic luster. By-products were primarily the binary iridium phosphide $IrP_2$ and in case of the dysprosium sample the ternary phosphide $Dy_7Ir_{17}P_{12}$ [32]. The $RE_5Ir_{19}P_{12}$ phosphides were obtained in the form of long needles or columns with lengths up to 200 μm. Based on a visual inspection of the product under a standard microscope, about 80% of the product mixtures consisted of the $RE_5Ir_{19}P_{12}$ phases. The $RE_5Ir_{19}P_{12}$, $IrP_2$, and $Dy_7Ir_{17}P_{12}$ crystals could clearly be distinguished on the basis of their crystal habit.

The whole series of the metal-rich phosphides $RE_5Ir_{19}P_{12}$ (*RE*=La–Nd, Sm–Lu) as well as the scandium and yttrium compounds can also be obtained via flux-free syntheses. However, varying synthesis routes had to be carried out.

Starting materials for the compounds $RE_5Ir_{19}P_{12}$ (*RE*=Sc, Y, La–Nd, Sm–Lu) were filings of the rare earth metals (Y, La–Pr, Tm, and Lu by Sigma Aldrich, 99.9%; Nd, Yb, and Sc by Smart Elements, 99.9%), pieces of samarium, europium, gadolinium, terbium, dysprosium, holmium, and erbium (Smart Elements, 99.9%), iridium powder (Heraeus, >99.9%), and red phosphorus (Hoechst, Knapsack, ultrapure). For the preparation of $RE_5Ir_{19}P_{12}$ (*RE*=Sc, Y, La–Nd, Tm–Lu) the elements were weighed in the ideal stoichiometric ratio 5:19:12 (*RE*:Ir:P), homogenized and pressed to a pellet. The latter were placed in tantalum crucibles, which were sealed in evacuated silica tubes. The samples were heated to 770 K at a rate of 20 K/h and kept at that temperature for 24 h in a muffle furnace. Subsequently the temperature was raised to 1370 K (Y, La–Ho, Yb), respectively 1470 K (Sc, Er, Tm, Lu) for another 24 h and the samples were cooled to room temperature within the furnace after the annealing program was finished. The inhomogeneous reaction products were carefully grinded, again pressed to pellets, placed in the tantalum crucibles and sealed in evacuated silica tubes. These were then positioned in a muffle furnace, which was heated to 1270 K (Y, La–Ho, Yb) or 1320 K (Sc, Er, Tm, Lu) for ten days. The samples were then cooled to room temperature within the furnace after the annealing sequence. This procedure was repeated six to ten times. However, regarding the compounds containing high melting rare earth metals like erbium, thulium, lutetium or scandium the process was continued up to sixteen times.

For the synthesis of the samarium and europium compound pieces of the rare earth metals were weighed with a 10% molar excess and positioned onto an iridium pellet in a tantalum tube. These tantalum tubes were sealed and placed in a water-cooled chamber of an induction furnace (Hüttinger Elektronik, Freiburg, Germany, Typ TIG 2.5/300). The temperature was raised to 1420 K for 1 h and then lowered to 1320 K for another 7 h. The power was switched off and the samples were cooled to room temperature within the furnace. The temperature was controlled by a Sensor Therm Methis MS09 pyrometer with an accuracy of ±30 K. No reaction with the container material was observed. After grinding carefully and weighing the samples, red phosphorus was added in ideal stoichiometric amounts. The mixtures were pressed to pellets, placed in tantalum crucibles, which were sealed in evacuated silica tubes and thermally treated in a muffle furnace as described above for $RE_5Ir_{19}P_{12}$ (*RE*=Sc, Y, La–Nd, Sm–Lu).

The phosphides $RE_5Ir_{19}P_{12}$ (*RE*=Gd–Er) could be obtained by arc-melting (ca. 700 mbar argon atmosphere) the ideal atomic ratios of pieces of the rare earth metals and pellets of pressed iridium powder. The argon was purified before by molecular sieves, silica gel, and titanium sponge (900 K). The rare earth–iridium buttons were then grinded carefully, the ideal amount of red phosphorus was added and the mixtures were homogenized and pressed to pellets. These were placed in tantalum crucibles, which were sealed in evacuated silica tubes. The samples were thermally treated in a muffle furnace as described above for $RE_5Ir_{19}P_{12}$ (*RE*=Sc, Y, La–Nd, Sm–Lu).

### 2.2. Scanning electron microscopy

The single crystals investigated on the diffractometer were studied by EDX using a Zeiss EVO MA10 scanning electron microscope with Sc, $LaB_6$, $CeO_2$, $DyF_3$, $ErF_3$, $TmF_3$, $YbF_3$, Ir and GaP as standards for the semiquantitative measurements. The analyses indicated Sc, La, Ce, Dy, Er, Tm, Yb, Ir, and P as main components. Due to the significant overlap of the phosphorus *K* (2.1013 keV) and iridium *M* (1.977 keV) lines, a quantitative analyses was not possible. In case of the cerium, erbium and thulium compound traces of the bismuth flux could be detected on the surface of the crystals. The remaining compounds did not show any impurity elements.

### 2.3. X-ray powder and single crystal data

All polycrystalline samples were characterized through Guinier powder patterns (imaging plate technique, Fujifilm BAS–1800) with Cu$K\alpha_1$ radiation and α-quartz ($a$=491.30 and $c$=540.46 pm) as an internal standard. The hexagonal lattice parameters (Table 1) were obtained from least-squares refinements of the powder data. To ensure proper indexing, the experimental patterns were compared to calculated ones [34] taking the atomic positions from the structure refinements. The powder lattice parameters compared well with the single crystal data.

Lath-shaped single crystals of $RE_5Ir_{19}P_{12}$ (*RE*=Sc, La, Ce, Dy, Er, Tm, Yb) were selected from the flux-grown samples. They were investigated by Laue photographs on a Buerger camera (white molybdenum radiation, Fuji-film image plate technique) in order to check the quality for intensity data collection. The data sets for *RE*=La, Dy, Er, and Tm were collected at room temperature by use of two four-circle diffractometers (CAD4) with graphite monochromatized Mo$K\alpha$ (71.073 pm) or Ag$K\alpha$ (56.086 pm) radiation and scintillation counters with pulse height discrimination. Scans were taken in the $\omega/2\theta$ mode. Empirical absorption corrections were applied on the basis of Ψ-scan data, accompanied by spherical absorption corrections. Alternatively numerical corrections have been carried out (see Tables 2 and 3). Intensity data of the crystals with *RE*=Sc, Ce, and Yb were collected at room temperature by use of a Stoe IPDS-II imaging plate diffractometer in oscillation mode (graphite monochromatized Mo$K\alpha$ radiation). Numerical absorption corrections were applied to the data sets. The $Sc_5Ir_{19}P_{12}$ crystal was additionally measured at 90 K. All relevant crystallographic data and details of the data collections and evaluations are listed in Tables 2 and 3.

**Table 1**
Lattice parameters (Guinier powder data) of the phosphides $RE_5Ir_{19}P_{12}$ (*RE*=Sc, Y, La–Nd, Eu–Lu).

| Compound | $a$ (pm) | $c$ (pm) | $V$ (nm$^3$) |
|---|---|---|---|
| $Sc_5Ir_{19}P_{12}$ | 1257.2(10) | 390.1(3) | 0.5340 |
| $Y_5Ir_{19}P_{12}$ | 1262.0(10) | 394.4(3) | 0.5439 |
| $La_5Ir_{19}P_{12}$ | 1271.7(9) | 402.0(3) | 0.5630 |
| $Ce_5Ir_{19}P_{12}$ | 1270.2(5) | 398.2(2) | 0.5564 |
| $Pr_5Ir_{19}P_{12}$ | 1269.1(5) | 397.3(2) | 0.5542 |
| $Nd_5Ir_{19}P_{12}$ | 1266.6(5) | 397.0(1) | 0.5516 |
| $Sm_5Ir_{19}P_{12}$ | 1266.1(6) | 396.1(2) | 0.5498 |
| $Eu_5Ir_{19}P_{12}$ | 1267.4(3) | 398.9(1) | 0.5549 |
| $Gd_5Ir_{19}P_{12}$ | 1262.9(3) | 395.7(1) | 0.5465 |
| $Tb_5Ir_{19}P_{12}$ | 1261.1(3) | 394.7(1) | 0.5436 |
| $Dy_5Ir_{19}P_{12}$ | 1260.1(7) | 394.2(3) | 0.5420 |
| $Ho_5Ir_{19}P_{12}$ | 1259.3(9) | 394.0(3) | 0.5411 |
| $Er_5Ir_{19}P_{12}$ | 1259.0(5) | 392.8(2) | 0.5392 |
| $Tm_5Ir_{19}P_{12}$ | 1258.5(8) | 392.7(3) | 0.5386 |
| $Yb_5Ir_{19}P_{12}$ | 1258.3(7) | 390.7(3) | 0.5357 |
| $Lu_5Ir_{19}P_{12}$ | 1257.5(10) | 390.5(3) | 0.5348 |

**Table 2**
Crystallographic data and structure refinements of $RE_5Ir_{19}P_{12}$ ($RE$=Sc, La, Ce, Dy).

| Refined composition | $Sc_5Ir_{19}P_{12}$ | $La_5Ir_{19}P_{12}$ | $Ce_5Ir_{18.0(1)}P_{12}$ | $Dy_5Ir_{19}P_{12}$ |
|---|---|---|---|---|
| Lattice parameters | Table 1 | Table 1 | Table 1 | Table 1 |
| Molar mass (g mol$^{-1}$) | 4248.24 | 4717.99 | 4537.61 | 4835.94 |
| Crystal size (μm$^3$) | 10 × 10 × 40 | 15 × 15 × 30 | 10 × 10 × 50 | 10 × 10 × 40 |
| Calculated density (g cm$^{-3}$) | 13.21 | 13.92 | 13.54 | 14.81 |
| Transmission (min/max) | 0.144/0.444 | 0.305/0.506 | 0.047/0.476 | 0.095/0.248 |
| Diffractometer type | IPDS-II | CAD4 | IPDS-II | CAD4 |
| Radiation (Å) | Mo (0.71073) | Ag (0.56086) | Mo (0.71073) | Mo (0.71073) |
| Detector distance (mm) | 80 | – | 90 | – |
| Exposure time (min) | 5 | – | 6 | – |
| $\omega$ range; increment (deg) | 0–180, 1.0 | – | 0–180, 1.0 | – |
| Integr. param. (A, B, EMS) | 12.8; 3.0; 0.012 | – | 13.0; 3.0; 0.014 | – |
| Absorption coeff. μ (mm$^{-1}$) | 120.2 | 66.1 | 118.1 | 133.9 |
| F(0 0 0) | 1748 | 1928 | 1858 | 1973 |
| $\theta$-range (deg.) | 3.2–31.8 | 2.5–28.0 | 1.8–30.4 | 3.2–30.1 |
| Range in $hkl$ | ±18, ±18, ±5 | ±21, +21, +6 | ±18, ±18, ±5 | ±17, ±17, ±5 |
| Total reflections | 5299 | 1853 | 4579 | 6240 |
| Independent reflections ($R_{(int)}$) | 734 (0.081) | 991 (0.060) | 680 (0.059) | 646 (0.118) |
| Refl. with $I \geq 2\sigma(I)$ ($R_{(sigma)}$) | 601 (0.082) | 691 (0.141) | 543 (0.065) | 581 (0.045) |
| Data / parameters | 734/38 | 991/38 | 680 / 40 | 646/38 |
| Goodness-of-fit | 0.742 | 0.572 | 0.790 | 1.174 $R$ |
| $R$ indices [$I \geq 2\sigma$(I)] | $R1$=0.030 | $R1$=0.029 | $R1$=0.024 | $R1$=0.029 |
| | $wR2$=0.036 | $wR2$=0.065 | $wR2$=0.046 | $wR2$=0.050 |
| $R$ indices (all data) | $R1$=0.042 | $R1$=0.055 | $R1$=0.036 | $R1$=0.037 |
| | $wR2$=0.037 | $wR2$=0.072 | $wR2$=0.048 | $wR2$=0.053 |
| Extinction coefficient | 0.00107(3) | 0.00140(4) | 0.00096(4) | 0.00063(6) |
| Larg. diff. peak / hole (eÅ$^{-3}$) | 2.77/−2.75 | 3.89/−4.15 | 2.27/−3.85 | 2.57/−5.49 |
| Absorption correction | Numerical | Numerical | Numerical | Numerical |
| Inversion twin ratio | 0.37(4) | 0.48(5) | 0.41(3) | 0.49(3) |

**Table 3**
Crystallographic data and structure refinements of $RE_5Ir_{19}P_{12}$ ($RE$=Er, Tm, Yb).

| Refined composition | $Er_5Ir_{19}P_{12}$ | $Tm_5Ir_{19}P_{12}$ | $Yb_5Ir_{19}P_{12}$ |
|---|---|---|---|
| Lattice parameters | Table 1 | Table 1 | Table 1 |
| Molar mass (g mol$^{-1}$) | 4859.74 | 4868.09 | 4888.64 |
| Crystal size (μm$^3$) | 15 × 15 × 30 | 10 × 15 × 30 | 10 × 10 × 60 |
| Calculated density (g cm$^{-3}$) | 14.97 | 15.01 | 15.15 |
| Transmission (min/max) | 0.448/0.978 | 0.456/0.740 | 0.010/0.708 |
| Diffractometer type | CAD4 | CAD4 | IPDS-II |
| Radiation | Mo (0.71073) | Mo (0.71073) | Mo (0.71073) |
| Detector distance (mm) | – | – | 80 |
| Exposure time (min) | – | – | 6 |
| $\omega$ range; increment (deg) | – | – | 0–180, 1.0 |
| Integr. param. (A, B, EMS) | – | – | 12.5; 2.8; 0.012 |
| Absorption coeff. μ (mm$^{-1}$) | 136.7 | 138.0 | 139.9 |
| F(0 0 0) | 1983 | 1988 | 1993 |
| $\theta$-range (deg.) | 3.2–30.1 | 3.2–35.2 | 3.2–29.9 |
| Range in $hkl$ | ±17, ±17, ±5 | ±20, ±20, ±6 | ±17, ±17, ±5 |
| Total reflections | 6332 | 9528 | 5827 |
| Independent reflections ($R_{(int)}$) | 644 (0.107) | 950 (0.104) | 636 (0.047) |
| Refl. with $I \geq 2\sigma(I)$ ($R_{(sigma)}$) | 597 (0.040) | 873 (0.037) | 602 (0.024) |
| Data/parameters | 644/38 | 950/38 | 636/37 |
| Goodness-of-fit | 1.138 | 1.105 | 0.979 |
| $R$ indices [$I \geq 2\sigma$(I)] | $R1$=0.024 | $R1$=0.023 | $R1$=0.017 |
| | $wR2$=0.045 | $wR2$=0.036 | $wR2$=0.029 |
| $R$ indices (all data) | $R1$=0.030 | $R1$=0.029 | $R1$=0.020 |
| | $wR2$=0.046 | $wR2$=0.038 | $wR2$=0.029 |
| Extinction coefficient | 0.00067(5) | 0.00062(3) | 0.00028(2) |
| Larg. diff. peak/hole (eÅ$^{-3}$) | 2.92/−4.75 | 3.45/−4.50 | 1.81/−1.80 |
| Absorption correction | Semiempirical | Semiempirical | Numerical |
| Flack parameter | – | – | 0.02(3) |
| Inversion twin ratio | 0.36(3) | 0.35(2) | – |

The Guinier patterns already indicated isotypism with $Sc_5Co_{19}P_{12}$ [8]. All seven data sets showed primitive hexagonal lattices and no further systematic extinctions, in agreement with space group $P6\bar{2}m$. The atomic positions of $Sc_5Co_{19}P_{12}$ [8] were taken as starting parameters and the structures were refined with SHELXL-97 [35,36] (full matrix least squares on $F_o^2$) with anisotropic displacement parameters for the metal and isotropic displacement parameters for the phosphorus atoms. The occupancy parameters have been refined in a separate series of least squares cycles. With the exception of the Ir1 and Ir5 sites of the cerium crystal, all sites were fully occupied within two standard deviations. These two iridium occupancy parameters were refined as least-squares variables in the final cycles, leading to the composition $Ce_5Ir_{18.0(1)}P_{12}$ for the investigated crystal.

**Table 4**
Atomic coordinates and equivalent isotropic displacement parameters ($pm^2$) for the phosphides $RE_5Ir_{19}P_{12}$ ($RE$=Sc, La, Ce, Dy, Er–Yb). $U_{eq}$ is defined as one third of the trace of the orthogonalized $U_{ij}$ tensor. $U_{13}=U_{23}=0$. The 2*e* Ir4 sites have only 50% occupancy (split position).

| Atom | Wyckoff site | *x* | *y* | *z* | $U_{11}$ | $U_{22}$ | $U_{33}$ | $U_{12}$ | $U_{eq}/U_{iso}$ |
|---|---|---|---|---|---|---|---|---|---|
| **$Sc_5Ir_{19}P_{12}$** | | | | | | | | | |
| Sc1 | 3*g* | 0.1818(8) | 0 | 1/2 | 218(24) | 205(41) | 128(37) | 102(21) | 185(16) |
| Sc2 | 2*c* | 1/3 | 2/3 | 0 | 97(20) | $U_{11}$ | 14(39) | 48(10) | 69(16) |
| Ir1 | 3*g* | 0.7188(1) | 0 | 1/2 | 116(4) | 40(5) | 55(6) | 20(3) | 79(3) |
| Ir2 | 6*j* | 0.19083(9) | 0.37026(8) | 0 | 53(4) | 54(4) | 41(4) | 35(3) | 46(2) |
| Ir3 | 6*k* | 0.1303(1) | 0.48964(9) | 1/2 | 47(4) | 61(4) | 56(5) | 38(3) | 50(2) |
| Ir4 | 2*e* | 0 | 0 | 0.0891(7) | | | | | 42(6) |
| Ir5 | 3*f* | 0.5480(1) | 0 | 0 | 80(4) | 117(6) | 80(7) | 59(3) | 89(3) |
| P1 | 3*f* | 0.8237(8) | 0 | 0 | | | | | 36(15) |
| P2 | 6*k* | 0.3153(7) | 0.4855(7) | 1/2 | | | | | 105(14) |
| P3 | 3*f* | 0.3598(8) | 0 | 0 | | | | | 60(15) |
| **$La_5Ir_{19}P_{12}$** | | | | | | | | | |
| La1 | 3*g* | 0.1864(2) | 0 | 1/2 | 51(6) | 40(9) | 64(11) | 20(4) | 53(4) |
| La2 | 2*c* | 1/3 | 2/3 | 0 | 50(6) | $U_{11}$ | 54(14) | 25(3) | 51(5) |
| Ir1 | 3*g* | 0.7125(1) | 0 | 1/2 | 59(4) | 45(6) | 61(7) | 22(3) | 57(3) |
| Ir2 | 6*j* | 0.1984(1) | 0.3782(1) | 0 | 68(4) | 46(4) | 48(4) | 29(4) | 54(2) |
| Ir3 | 6*k* | 0.1285(1) | 0.4904(1) | 1/2 | 55(4) | 50(4) | 62(5) | 25(4) | 56(2) |
| Ir4 | 1*a* | 0 | 0 | 0 | 43(7) | $U_{11}$ | 89(12) | 21(3) | 58(5) |
| Ir5 | 3*f* | 0.5413(2) | 0 | 0 | 89(5) | 151(8) | 106(8) | 76(4) | 109(3) |
| P1 | 3*f* | 0.8192(10) | 0 | 0 | | | | | 73(19) |
| P2 | 6*k* | 0.3114(8) | 0.4819(8) | 1/2 | | | | | 69(13) |
| P3 | 3*f* | 0.3638(11) | 0 | 0 | | | | | 120(22) |
| **$Ce_5Ir_{18.0(1)}P_{12}$** | | | | | | | | | |
| Ce1 | 3*g* | 0.8140(2) | 0 | 1/2 | 49(6) | 53(10) | 38(11) | 27(5) | 46(4) |
| Ce2 | 2*c* | 2/3 | 1/3 | 0 | 50(7) | $U_{11}$ | 25(16) | 25(4) | 42(6) |
| Ir1[a] | 3*g* | 0.2863(1) | 0 | 1/2 | 44(6) | 40(8) | 24(8) | 20(4) | 36(5) |
| Ir2 | 6*j* | 0.8023(1) | 0.6229(1) | 0 | 59(5) | 46(5) | 37(5) | 30(4) | 46(2) |
| Ir3 | 6*k* | 0.8711(1) | 0.5110(1) | 1/2 | 51(5) | 53(5) | 26(6) | 30(4) | 42(2) |
| Ir4 | 2*e* | 0 | 0 | 0.022(2) | | | | | 32(7) |
| Ir5[a] | 3*f* | 0.4553(2) | 0 | 0 | 91(10) | 123(11) | 60(12) | 61(6) | 88(7) |
| P1 | 3*f* | 0.1801(9) | 0 | 0 | | | | | 66(18) |
| P2 | 6*k* | 0.6867(7) | 0.5170(7) | 1/2 | | | | | 66(14) |
| P3 | 3*f* | 0.6331(9) | 0 | 0 | | | | | 108(20) |
| **$Dy_5Ir_{19}P_{12}$** | | | | | | | | | |
| Dy1 | 3*g* | 0.1844(1) | 0 | 1/2 | 63(5) | 44(7) | 21(8) | 22(3) | 45(3) |
| Dy2 | 2*c* | 1/3 | 2/3 | 0 | 45(5) | $U_{11}$ | 32(11) | 22(2) | 41(4) |
| Ir1 | 3*g* | 0.7172(1) | 0 | 1/2 | 68(4) | 38(5) | 28(6) | 19(3) | 48(2) |
| Ir2 | 6*j* | 0.19436(9) | 0.37368(9) | 0 | 55(4) | 56(4) | 15(4) | 37(3) | 38(2) |
| Ir3 | 6*k* | 0.12810(9) | 0.48809(8) | 1/2 | 43(4) | 51(4) | 15(4) | 24(3) | 36(2) |
| Ir4 | 2*e* | 0 | 0 | 0.0322(14) | | | | | 45(6) |
| Ir5 | 3*f* | 0.5485(1) | 0 | 0 | 77(4) | 110(6) | 39(6) | 55(3) | 72(3) |
| P1 | 3*f* | 0.8209(7) | 0 | 0 | | | | | 60(16) |
| P2 | 6*k* | 0.3137(6) | 0.4829(6) | 1/2 | | | | | 70(12) |
| P3 | 3*f* | 0.3643(7) | 0 | 0 | | | | | 72(16) |
| **$Er_5Ir_{19}P_{12}$** | | | | | | | | | |
| Er1 | 3*g* | 0.1841(1) | 0 | 1/2 | 76(4) | 36(5) | 36(7) | 18(3) | 54(3) |
| Er2 | 2*c* | 1/3 | 2/3 | 0 | 43(4) | $U_{11}$ | 25(8) | 22(2) | 37(3) |
| Ir1 | 3*g* | 0.71742(9) | 0 | 1/2 | 68(3) | 24(4) | 12(4) | 12(2) | 39(2) |
| Ir2 | 6*j* | 0.19372(7) | 0.37324(7) | 0 | 39(3) | 40(3) | 16(3) | 23(3) | 30(2) |
| Ir3 | 6*k* | 0.12855(7) | 0.48825(7) | 1/2 | 35(3) | 39(3) | 15(3) | 20(3) | 29(2) |
| Ir4 | 2*e* | 0 | 0 | 0.0457(8) | | | | | 29(5) |

| | | | | | | | | | |
|---|---|---|---|---|---|---|---|---|---|
| Ir5 | 3f | 0.54851(9) | 0 | 0 | 65(3) | 100(5) | 38(5) | 50(2) | 64(2) |
| P1 | 3f | 0.8218(6) | 0 | 0 | | | | | 42(13) |
| P2 | 6k | 0.3129(5) | 0.4826(5) | 1/2 | | | | | 67(10) |
| P3 | 3f | 0.3631(6) | 0 | 0 | | | | | 69(13) |
| **$Tm_5Ir_{19}P_{12}$** | | | | | | | | | |
| Tm1 | 3g | 0.81533(7) | 0 | 1/2 | 54(2) | 35(3) | 52(4) | 18(2) | 49(1) |
| Tm2 | 2c | 2/3 | 1/3 | 0 | 45(2) | $U_{11}$ | 54(5) | 23(1) | 48(2) |
| Ir1 | 3g | 0.28086(6) | 0 | 1/2 | 49(2) | 27(3) | 31(3) | 14(1) | 38(1) |
| Ir2 | 6j | 0.80658(5) | 0.62687(5) | 0 | 36(2) | 37(2) | 41(2) | 25(2) | 35(1) |
| Ir3 | 6k | 0.87214(5) | 0.51251(5) | 1/2 | 34(2) | 38(2) | 40(2) | 20(2) | 36(1) |
| Ir4 | 2e | 0 | 0 | 0.9695(7) | | | | | 38(3) |
| Ir5 | 3f | 0.44887(6) | 0 | 0 | 41(2) | 63(3) | 51(3) | 32(1) | 49(1) |
| P1 | 3f | 0.1775(4) | 0 | 0 | | | | | 43(8) |
| P2 | 6k | 0.6870(4) | 0.5178(4) | 1/2 | | | | | 75(6) |
| P3 | 3f | 0.6355(4) | 0 | 0 | | | | | 88(9) |
| **$Yb_5Ir_{19}P_{12}$** | | | | | | | | | |
| Yb1 | 3g | 0.81639(8) | 0 | 1/2 | 123(3) | 69(4) | 50(3) | 35(2) | 87(2) |
| Yb2 | 2c | 2/3 | 1/3 | 0 | 66(3) | $U_{11}$ | 47(4) | 33(2) | 60(2) |
| Ir1 | 3g | 0.28377(7) | 0 | 1/2 | 93(2) | 48(4) | 35(2) | 24(2) | 64(1) |
| Ir2 | 6j | 0.80647(6) | 0.62691(5) | 0 | 67(2) | 62(2) | 35(2) | 40(2) | 51(1) |
| Ir3 | 6k | 0.87040(6) | 0.51078(6) | 1/2 | 54(3) | 67(2) | 39(2) | 32(2) | 53(1) |
| Ir4 | 2e | 0 | 0 | 0.9384(3) | | | | | 57(4) |
| Ir5 | 3f | 0.45392(7) | 0 | 0 | 94(3) | 134(4) | 66(3) | 67(2) | 94(2) |
| P1 | 3f | 0.1774(4) | 0 | 0 | | | | | 75(9) |
| P2 | 6k | 0.6862(4) | 0.5158(4) | 1/2 | | | | | 87(7) |
| P3 | 3f | 0.6392(4) | 0 | 0 | | | | | 75(8) |

[a] Ir1 and Ir5 sites are occupied by 95.9(4)% and 73.4(4)%, respectively.

**Table 5**
Interatomic distances /pm of $La_5Ir_{19}P_{12}$. All distances within the first coordination spheres are listed.

| | | | | | | | |
|---|---|---|---|---|---|---|---|
| La1: | 2 | P3 | 302(1) | Ir4: | 3 | P1 | 230(1) |
| | 4 | P1 | 308.2(5) | | 6 | La1 | 310.8(3) |
| | 2 | Ir4 | 310.8(3) | Ir5: | 1 | P3 | 226(1) |
| | 4 | Ir2 | 319.4(2) | | 4 | Ir3 | 286.1(2) |
| | 2 | Ir1 | 321.3(3) | | 4 | P2 | 286.2(6) |
| | 2 | Ir3 | 336.1(4) | | 2 | Ir2 | 293.6(3) |
| La2: | 6 | P2 | 299.7(6) | | 2 | Ir1 | 296.3(2) |
| | 6 | Ir3 | 316.4(2) | P1: | 1 | Ir4 | 230(1) |
| | 3 | Ir2 | 317.9(3) | | 2 | Ir2 | 240.7(8) |
| Ir1: | 2 | P2 | 233.5(9) | | 2 | Ir1 | 242.5(7) |
| | 2 | P1 | 242.5(7) | | 4 | La1 | 308.2(5) |
| | 4 | Ir2 | 282.2(2) | P2: | 1 | Ir3 | 230.1(9) |
| | 2 | Ir5 | 296.3(2) | | 1 | Ir1 | 233.6(9) |
| | 2 | La1 | 321.3(3) | | 1 | Ir3 | 238.2(9) |
| Ir2: | 1 | P1 | 240.7(8) | | 2 | Ir2 | 243.9(5) |
| | 1 | P3 | 243.6(6) | | 2 | Ir5 | 286.2(6) |
| | 2 | P2 | 243.9(5) | | 2 | La2 | 299.7(6) |
| | 2 | Ir1 | 282.2(2) | P3: | 1 | Ir5 | 226(1) |
| | 2 | Ir3 | 285.2(2) | | 2 | Ir2 | 243.6(6) |
| | 1 | Ir5 | 293.6(3) | | 4 | Ir3 | 258.3(4) |
| | 1 | La2 | 317.9(3) | | 2 | La1 | 302(1) |
| | 2 | La1 | 319.4(2) | | | | |
| Ir3: | 1 | P2 | 230.1(9) | | | | |
| | 1 | P2 | 238.2(9) | | | | |
| | 2 | P3 | 258.3(4) | | | | |
| | 1 | Ir3 | 282.9(3) | | | | |
| | 2 | Ir2 | 285.2(2) | | | | |
| | 2 | Ir5 | 286.1(2) | | | | |
| | 2 | La2 | 316.4(2) | | | | |
| | 1 | La1 | 336.1(4) | | | | |

For $La_5Ir_{19}P_{12}$ all anisotropic displacement parameters were well behaved. The Ir4 sites of all other crystals showed extremely high $U_{33}$ parameters, indicating a violation of the mirror plane. For these sites we have introduced split positions 0, 0, *z* instead of 0, 0, 0 (with isotropic displacement parameters), as already observed for the prototype $Sc_5Co_{19}P_{12}$ [8], $Ho_5Co_{19}P_{12}$ [10], and $Zr_5Co_{19}P_{12}$ [20]. The crystal chemical consequences are discussed below. Final difference Fourier synthesis revealed no significant residual peaks. The refined atomic parameters and interatomic distances (exemplarily for $La_5Ir_{19}P_{12}$) are listed in Tables 4 and 5.

Further details on the structure refinements are available. Details may be obtained from: Fachinformationszentrum Karlsruhe, D-76344 Eggenstein–Leopoldshafen (Germany), by quoting the Registry No's. CSD–422911 ($Sc_5Ir_{19}P_{12}$), CSD–422912 ($La_5Ir_{19}P_{12}$), CSD–422913 ($Ce_5Ir_{18.0(1)}P_{12}$), CSD–422914 ($Dy_5Ir_{19}P_{12}$), CSD–422915 ($Er_5Ir_{19}P_{12}$), CSD–422916 ($Tm_5Ir_{19}P_{12}$), and CSD–422917 ($Yb_5Ir_{19}P_{12}$).

## 3. Result and discussion

### 3.1. Crystal chemistry

The iridium-rich phosphides $RE_5Ir_{19}P_{12}$ (*RE*=Sc, Y, La–Nd, Eu–Lu) crystallize with the hexagonal $Sc_5Co_{19}P_{12}$ [8] type structure. The cell volumes (Table 1 and Fig. 1) decrease from the lanthanum to the lutetium compound as expected from the lanthanoid contraction. The $Y_5Ir_{19}P_{12}$ volume fits between the gadolinium and the terbium compound. $Eu_5Ir_{19}P_{12}$ has a slightly higher cell volume, indicating a tendency towards divalent europium. So far we not got enough single crystals of this phosphide to perform magnetic susceptibility measurements and $^{151}$Eu Mössbauer spectroscopy for determination of the exact europium valence. Also with the smallest rare earth element scandium we obtained an isotypic compound. The cell volume is close to the one of $Lu_5Ir_{19}P_{12}$.

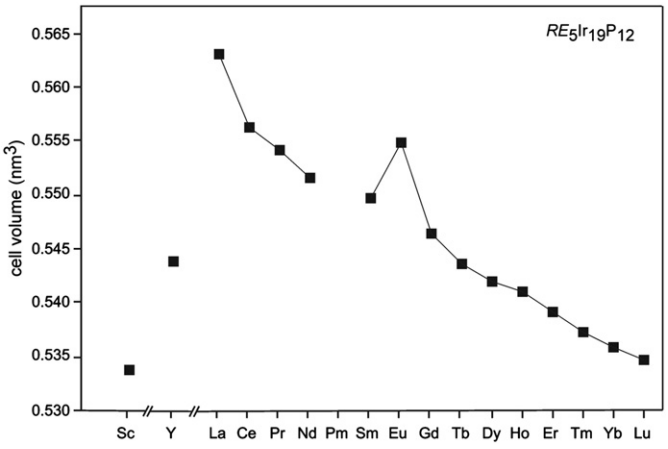


**Fig. 1.** Trend of the unit cell volumes in the series $RE_5Ir_{19}P_{12}$.

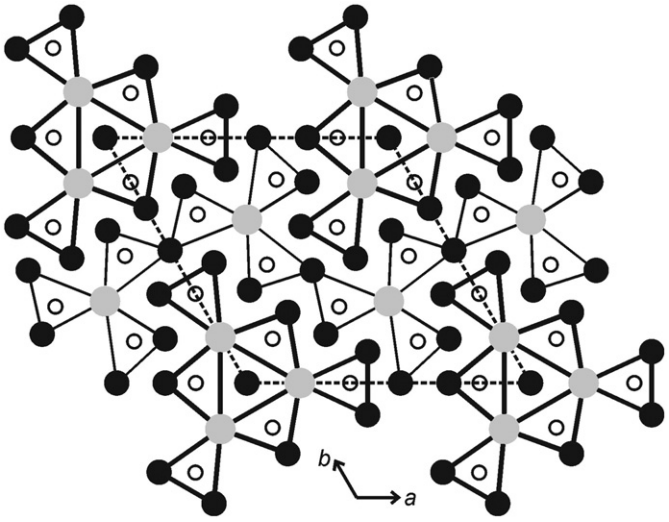


**Fig. 2.** Projection of the $La_5Ir_{19}P_{12}$ structure along the short unit cell axis. All atoms lie on mirror planes at $z=0$ (thin lines) and $z=1/2$ (thick lines). Lanthanum, iridium, and phosphorus atoms are drawn as medium gray, filled, and open circles, respectively. The trigonal prismatic building units are emphasized.

Due to the low phosphorus content we observe no P–P contacts in the $RE_5Ir_{19}P_{12}$ phosphides. In the following we exemplarily discuss the $La_5Ir_{19}P_{12}$ structure in more detail. A projection of the unit cell is presented in Fig. 2. The three crystallographically independent phosphorus sites all have coordination number nine in tricapped trigonal prismatic coordination. This is the typical coordination in most metal-rich phosphide structures. The distorted trigonal prisms are condensed via common edges in the *xy* plane, leading to the propeller-like motifs (Fig. 2). The two different building units of condensed distorted trigonal prisms are shifted by half a translation period *c*. These building units are further condensed along the *c* axis via common triangular faces. The P centered trigonal prisms around the origin form a regular $La_6$ prism, which is centered by the Ir4 atoms. This description of the structure is a purely geometrical one, however this type of description is very helpful in distinguishing many structure types [1–5] of metal-rich phosphides and related compounds.

The shortest interatomic distances in the $La_5Ir_{19}P_{12}$ structure occur for Ir–P with a range from 230 to 286 pm. Each of the five crystallographically independent iridium atoms has at least one short Ir–P distance, which is close to the sum of the covalent radii [37] of 236 pm, indicating substantial covalent Ir–P bonding. Together the iridium and phosphorus atoms build up a three-dimensional $[Ir_{19}P_{12}]$ network which leaves larger, slightly distorted hexagonal prismatic cavities that are filled by La1 and La2 (Fig. 3). These cavities are build up by 16 (6P+10Ir) and 15 (6P+9Ir) atoms, respectively. Although the $[Ir_{19}P_{12}]$ network seems to be complex at first sight, it can be described as an intergrowth of slabs of simpler structure types, similar to the recently reported iridium-rich $RE_xIr_yP_z$ phosphides [28–32]. As outlined in Fig. 3, the $La_5Ir_{19}P_{12}$ structure is an intergrowth of slightly distorted $ThCr_2Si_2$ ($BaIr_2P_2$ [38] and SrPtSb type slabs. SrPtSb is an ordered version of $AlB_2$ and occurs also for the series of *RE*PtP phosphides [39].

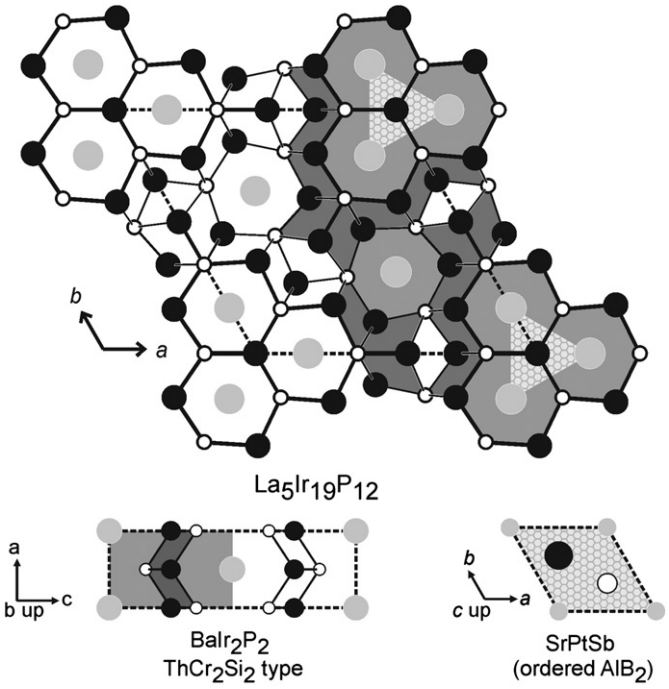


**Fig. 3.** Projection of the $La_5Ir_{19}P_{12}$ structure onto the *xy* plane. All atoms lie on mirror planes at $z=0$ (thin lines) and $z=1/2$ (thick lines). Lanthanum, iridium, and phosphorus atoms are drawn as medium gray, filled, and open circles, respectively. The three-dimensional $[Ir_{19}P_{12}]$ network is emphasized. The right-hand part of the drawing highlights the intergrowth character of $ThCr_2Si_2$ ($BaIr_2P_2$) and SrPtSb (ordered $AlB_2$) related slabs by different shadings.

Within the three-dimensional $[Ir_{19}P_{12}]$ network the Ir1, Ir2, Ir3, and Ir5 atoms have between 5 and 8 iridium neighbors at Ir–Ir distances ranging from 282 to 296 pm, slightly longer than in *fcc* iridium [40], where each iridium atom has twelve iridium neighbors at 272 pm. Only the Ir4 atoms show no Ir–Ir bonding. This is almost similar to the series of $RE_7Ir_{17}P_{12}$ phosphides [32]. The iridium substructure of $La_5Ir_{19}P_{12}$ is presented in Fig. 4. With the same composition $Th_5Fe_{19}P_{12}$ [22] and $Yb_5Ni_{19}P_{12}$ [23] have been reported, however, these phosphides have a completely different crystal structure. For comparison, the iron substructure of $Th_5Fe_{19}P_{12}$ [22] is also shown.

Finally we recur to the displacements of the Ir4 sites. Only in $La_5Ir_{19}P_{12}$ with the largest lattice parameters this site is well behaved. Already in $Ce_5Ir_{19}P_{12}$ the Ir4 site shows a severe displacement off the mirror plane and we refined this site with a split position 0, 0, 0.022 instead of 0, 0, 0 and an isotropic displacement parameter. This split model was applied to all other data sets with the smaller rare earth elements. The most pronounced Ir4 displacement of 0.0891 occurs for $Sc_5Ir_{19}P_{12}$, leading to a distance of 69 pm between the two split positions. A similar situation has been observed for $Sc_5Co_{19}P_{12}$ [8], $Ho_5Co_{19}P_{12}$ [10], and $Zr_5Co_{19}P_{12}$ [20] and is indicative of static disorder. An increase of the displacement with decreasing size of the rare

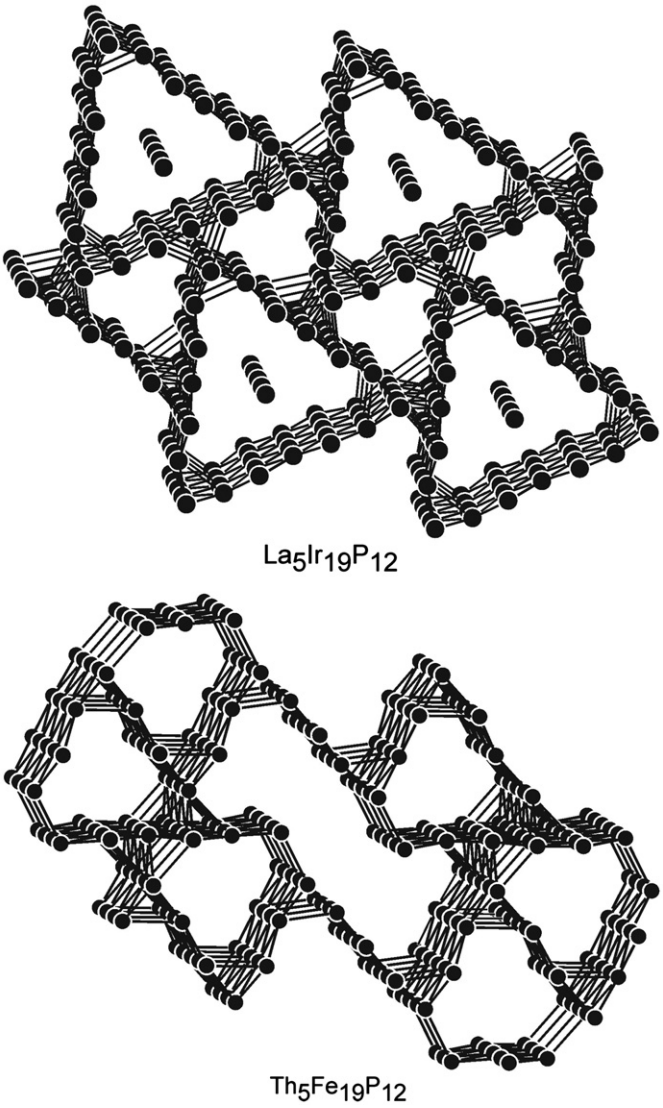


**Fig. 4.** Iridium and iron substructures in hexagonal $La_5Ir_{19}P_{12}$ and monoclinic $Th_5Fe_{19}P_{12}$ (views along the hexagonal and monoclinic axes).

earth element also occurs for the rhodium centered rare earth prisms for the *RE*RhSn stannides with the smaller rare earth elements [41].

In order to check for a potential displacive phase transition, we have also measured the $Sc_5Ir_{19}P_{12}$ crystal (the one with the largest displacement) at 90 K. The image plate data gave no hint for superstructure reflections nor for diffuse streaks, similar to the situation in $M_{5+x}Mg_{18-x}E_{13}$ ($M$=Sr, Ba; $E$=Si, Ge) [25]. Thus, the only possibility for an ordering of the Ir4 atoms can be a *translationengleiche* symmetry reduction. Temperature dependent investigations of the displacement parameters, especially of the $U_{33}$ parameter for the Ir4 site, could give further hints about a phase transition.

An alternative refinement is the use of an anharmonic tensor for the displacement of the Ir4 atom. Already a tensor of fourth grade sufficiently describes the Ir4 position (0 0 0). Fourier-transformation of the displacement parameters provides a *p.d.f.* map (probability density function) for the Ir4 position, which clearly shows a double maximum for the probability density, i. e. on either side of the mirror plane, but with a continuous probability between the maxima. At 90 K this dumbbell shaped tensor still shows a positive probability on the connecting line of the maxima indicating that the possible phase transition still has not taken place.

A very useful complementary tool for superstructure determination is $^{45}$Sc solid state NMR spectroscopy [42]. We have recently unambiguously determined the ScAgSn [43] superstructure by a combination of $^{45}$Sc solid state NMR spectroscopy and single crystal X-ray diffraction. For $Sc_5Ir_{19}P_{12}$ we can additionally use the $^{31}$P nucleus for further experiments. Synthesis of sufficient single phase material for these spectroscopic studies is in progress.

## Acknowledgments

This work was financially supported by the Deutsche Forschungsgemeinschaft.

## References

[1] Yu. Kuz'ma, S.Chykhrij Phosphides, in: K.A. Gschneidner Jr., L. Eyring (Eds.), Handbook on the Physics and Chemistry of Rare Earths, vol. 23, Elsevier Science, Amsterdam, 1996, pp. 285–433 Chapter 156.
[2] J.Y. Pivan, R. Guérin, J. Solid State Chem. 135 (1998) 218.
[3] S.I. Chykhrij, Pol. J. Chem. 73 (1999) 1595.
[4] C. Le Sénéchal, V.S. Babizhetsky, S. Députier, J.-Y. Pivan, R. Guérin, Z. Anorg. Allg. Chem. 627 (2001) 1325.
[5] R. Pöttgen, W. Hönle, H.G. von Schnering, in: Phosphides: Solid State Chemistry, in R.B. King (Ed.), Encyclopedia of Inorganic Chemistry, vol. VII, 2nd ed., Wiley, New York, 2005, pp. 4255–4308.
[6] J.-Y. Pivan, R. Guérin, M. Sergent, J. Solid State Chem. 68 (1987) 11.
[7] Yu.M. Prots', W. Jeitschko, Inorg. Chem. 37 (1998) 5431.
[8] W. Jeitschko, E.J. Reinbold, Z. Naturforsch. 40b (1985) 900.
[9] J.Y. Pivan, R. Guérin, M. Sergent, Inorg. Chim. Acta 109 (1985) 221.
[10] U. Jakubowski-Ripke, W. Jeitschko, J. Less-Common Met. 136 (1988) 261.
[11] S.I. Chikhrii, Yu.B. Kuz'ma, Russ. J. Inorg. Chem. 35 (1990) 1821.
[12] S.V. Oryshchyn, S.I. Chykhrij, V.S. Babizhetsky, Y.B. Kuz'ma, Dopov. Akad. Nauk. Ukr. RSR 6 (1991) 138.
[13] V.S. Babizhetskii, S.I. Chikhrii, S.V. Oryshchyn, Y.B. Kuz'ma, Ukr. Khim. Zh. 59 (1993) 240.
[14] R.J. Cava, T. Siegrist, S.A. Carter, J.J. Krajewski, W.F. Peck Jr., H.W. Zandbergen, J. Solid State Chem. 121 (1996) 51.
[15] H.W. Zandbergen, J. Jansen, J. Micr. 190 (1998) 222.
[16] J. Jansen, D. Tang, H.W. Zandbergen, H. Schenk, Acta Crystallogr. A54 (1998) 91.
[17] S.V. Orishin, O.V. Zhak, I.V. Koval'chuk, Y.B. Kuz'ma, Russ. J. Inorg. Chem. 46 (2001) 1892.
[18] R.O. Demchyna, S.V. Oryshyn, Yu.B. Kuz'ma, J. Alloys Compd. 322 (2001) 176.
[19] S. Budnyk, Yu.B. Kuz'ma, Polish J. Chem. 76 (2002) 1553.
[20] V. Ghetta, P. Chaudouet, R. Madar, J.P. Senateur, B. Lambert-Andron, J. Less-Common Met. 120 (1986) 197.
[21] A. Wurth, A. Löhken, A. Mewis, Z. Anorg. Allg. Chem. 628 (2002) 661.
[22] J.H. Albering, W. Jeitschko, Z. Naturforsch. 47b (1992) 1521.
[23] S. Budnyk, S.I. Chikhrii, Yu.B. Kuz'ma, Collection of abstracts, in: Proceedings of the Seventh International Conference on the Crystal Chemistry of Intermetallic Compounds, Lvov, Ukraine, 1999, PA6.
[24] S.J. Steinwand, W.-M. Hurng, J.D. Corbett, J. Solid State Chem. 94 (1991) 36.
[25] R. Nesper, S. Wengert, F. Zürcher, A. Currao, Chem. Eur. J. 5 (1999) 3382.
[26] F. Kubel, H. Hagemann, H. Bill, Z. Anorg. Allg. Chem. 622 (1996) 343.
[27] F. Kubel, H. Hagemann, H. Bill, Z. Anorg. Allg. Chem. 622 (1996) 1374.
[28] U. Pfannenschmidt, U.Ch. Rodewald, R. Pöttgen, Z. Anorg. Allg. Chem. 636 (2010) 314.
[29] U. Pfannenschmidt, U.Ch. Rodewald, R. Pöttgen, Z. Kristallogr. 225 (2010) 280.
[30] U. Pfannenschmidt, U.Ch. Rodewald, R. Pöttgen, Z. Naturforsch. 66b (2011) 7.
[31] U. Pfannenschmidt, U.Ch. Rodewald, R. Pöttgen, Z. Kristallogr. 226 (2011) 229.
[32] U. Pfannenschmidt, R. Pöttgen, Intermetallics 19 (2011) 1052.
[33] M.G. Kanatzidis, R. Pöttgen, W. Jeitschko, Angew. Chem. 117 (2005) 7156; M.G. Kanatzidis, R. Pöttgen, W. Jeitschko, Angew. Chem. Int. Ed. 44 (2005) 6996.
[34] K. Yvon, W. Jeitschko, E. Parthé, J. Appl. Crystallogr. 10 (1977) 73.
[35] G.M. Sheldrick, SHELXL-97–A Program for Crystal Structrue Refinement, University of Göttingen, Germany, 1997.
[36] G.M. Sheldrick, Acta Crystallogr. A64 (2008) 112.
[37] J. Emsley, The Elements, Oxford University Press, Oxford, 1999.
[38] A. Löhken, C. Lux, D. Johrendt, A. Mewis, Z. Anorg. Allg. Chem. 628 (2002) 1472.
[39] G. Wenski, A. Mewis, Z. Kristallogr. 176 (1986) 125.
[40] J. Donohue, The Structures of the Elements, Wiley, New York, U.S.A, 1974.
[41] R. Mishra, R. Pöttgen, R.-D. Hoffmann, H. Trill, B.D. Mosel, H. Piotrowski, M.F. Zumdick, Z. Naturforsch. 56b (2001) 589.
[42] H. Eckert, R. Pöttgen, Z. Anorg. Allg. Chem. 636 (2010) 2232.
[43] C.P. Sebastian, L. Zhang, C. Fehse, R.-D. Hoffmann, H. Eckert, R. Pöttgen, Inorg. Chem. 46 (2007) 771.